Next Energy 1 (2023) 100020

Contents lists available at ScienceDirect

Next Energy

journal homepage: www.sciencedirect.com/journal/next-energy

Research article

Dynamic performance simulation of combined gas electric and steam power plants for cruise-ferry ships

Alessandro Dotto*,[1], Riccardo Sacchi, Francesca Satta, Ugo Campora

DIME, University of Genoa, via Montallegro 1, 16145 Genoa, Italy

ARTICLE INFO

Keywords:
Ship power plants
Dynamic simulation of combined cycle power plants
Liquefied Natural Gas propulsion
Emission reduction
COGES

ABSTRACT

This work aims at investigating the feasibility of COmbined Gas Electric and Steam (COGES) plants onboard Liquefied Natural Gas (LNG) fueled ships, by means of a novel, flexible tool. Firstly, the nominal operating conditions of 6 commercially available gas turbines (GTs) as well as their dynamic performance are simulated. Secondly, 6 different integrated COGES-reciprocating engine power plants are assembled and compared in terms of cogeneration efficiency within an optimized repowering study for the cruise-ferry ship GNV La Suprema. The optimization accounts for variable ship speed, season and GT control strategy for an overall number of 264 operating conditions considered. Thirdly, the time-dependent performance of the best COGES plant is assessed under actual navigation conditions for La Suprema. Overall, the results show the great potential of combining COGES plants with reciprocating engines for the marine sector. In particular, in the ship speed range centered around the actual cruise speed for La Suprema (i.e. 22 knots), all the COGES plants are able to cover the propulsion and hotel power demands more efficiently than reciprocating engines, with a 1–5 % benefit on cogeneration efficiency. Overall, a 51 % maximum cogeneration efficiency is found to be provided by COGES plants based on LM2500 and TITAN250 gas turbines.

1. Introduction

More and more stringent regulations concerning pollutant and greenhouse gas (GHG) emissions from ship power plants have been introduced within the maritime sector in the last few decades. International Maritime Organization (IMO) imposed basic limits for sulphur oxides (SO_x) and nitrogen oxides (NO_x) worldwide [1,2], whereas more restrictive limitations exist in the Emission Control Areas (ECA). Within a few years, Mediterranean Sea as well as East and West Coast of North America, Baltic and North Seas are supposed to be included in the ECA zones. In the effort to cope with environmental regulations, the scientific community attention is mainly focused on two strategies: replacing traditional oils (HFO and MDO) with alternative fuels capable to guarantee lower emissions, and increasing the overall power plant efficiency. Where the first strategy is concerned, LNG is presently evaluated as a clean fuel for ship propulsion [3,4] as it significantly reduces emission when compared to HFO. The primary environmental advantages of using LNG instead of HFO consist in no SO_x production, up to 85 % reduction of NO_x emissions and 25–30 % reduction of CO_2 [5,6]. On the other hand, the installation of prime movers equipped with waste heat recovery systems to produce further electrical power [7–9] and the replacement of conventional mechanical propulsion plant with integrated electric layout are part of the strategy aimed at improving the energy savings [10]. In this paper both strategies have been considered. Specifically, the dynamic performance of a COmbined Gas Electric and Steam (COGES) plant fueled by LNG is investigated in a repowering study for the cruise-ferry ship GNV La Suprema. Combining a gas turbine (GT) with a bottoming steam power cycle is an option commonly used in terrestrial power plants due to its high electrical efficiency [11]. The pioneering work of Merz and Pakula [12] concerning COGES plants applied to the marine sector showed their benefits in terms of low environmental impact, reduced fuel consumption rate and increased operational flexibility. Haglind [13] applied COGES propulsion plants to container ships, tankers and bulk carriers, while successive works investigated it for large container ships [14]. The typical high power-to-weight ratio characterizing gas turbines made them widely used onboard military ships [15,16]. The benefits of COGES plants in terms of cogeneration efficiency have been demonstrated also for small GT sizes in Barsi et al. [17,18] in the application onboard medium size cruise and Ropax ships. Despite the compactness

* Corresponding author.
E-mail address: alessandro.dotto@edu.unige.it (A. Dotto).
[1] 0000-0002-2207-4372

https://doi.org/10.1016/j.nxener.2023.100020
Received 25 November 2022; Received in revised form 10 March 2023; Accepted 9 April 2023

Nomenclature

P	Power, W
p	Pressure, Pa
ϵ	Expansion ratio
LHV	Lower Heating Value, J/kg
x	Steam quality
$\dot{m}$	Mass flow, kg/s
η_{el}	Electrical efficiency
θ	IGV opening angle
η_g	Cogeneration efficiency
β	Pressure ratio
T	Temperature, K
$\dot{q}$	Specific heat flux, W/m^2
e	Error
U	Flow velocity, m/s
V	Volume, m^3
n	Normal vector
A	Surface area, m^2
$\tilde{E}$	Energy, J
$\tilde{e}$	Specific energy, J/kg
S	Entropy, $J/(kgK)$
H	Enthalpy, J/kg
m	Mass, kg
N	Rotational speed, rpm
f	Air to fuel ratio
ρ	Density, kg/m^3
P_b	Brake power, W
P_o	Propeller power, W
COGES	COmbined Gas Electric and Steam
GT	Gas Turbine
GGS	Gas Generator Shaft
PAR	Partialization
P	Known parameters
X	Optimization variables
DF	Dual-Fuel engine
HRSG	Heat Recovery Steam Generator
WHR	Waste Heat Recovery
ST	Steam Turbine
ST	Steam Turbine
EG	Electrical Generator
EM	Electrical Motor
O	Objective
C	Constraints
LNG	Liquefied Natural Gas
HFO	Heavy Fuel Oil
MDO	Marine Diesel Oil
GP	Genoa-Palermo
GB	Genoa-Barcelona
NP	Naples-Palermo
NC	Naples-Catania
TIT	Gas Turbine Inlet Temperature, K
TOT	Gas Turbine Outlet Temperature, K
IGV	Inlet Guide Vane
MOGA	Multi-Objective Genetic Algorithm
SL	Surge limit
CV	Control volume
CS	Control surface
EVA	Evaporator
SH	Superheater
ECO	Economizer
COND	Condenser
sea	Sea water
a	Ambient
R	Reference value
ex	Exhaust gas
net	Net
in	Inlet value
el	Electrical
th	Thermal
mec	Mechanical
c	Compressor
t	Turbine
TGG	Gas generator turbine
PT	Power turbine
eq	Equivalent
sat	Saturation value
i	Inlet value
o	Outlet value
w	Water
s	Steam
cc	Combustion chamber
f	Fuel

of GT guarantees more volume and weight available for passengers or freights, only few cruise ships powered by COGES plants were built for the civil maritime sector (i.e. Millennium and Infinity from Celebrity or Radiance of the Seas from the Royal Caribbean). Nevertheless, fuel flexibility of GTs as well as the energetic and environmental benefits provided by COGES plants are recently gaining attention to enable energy transition in the marine field. In a previous work [10], the authors showed that installing COGES plants onboard cruise-ferries can improve ship performances by both energetic and environmental point of views, owing to their higher cogeneration efficiency and lower CO_2 emissions in comparison to Dual-Fuel (DF) engines. Furthermore, the economic feasibility of COGES during actual ship speed navigation conditions was proved in the same work, with reduced operational costs achieved over a broad ship speed range and comparable investments with respect to DF engines. To get a more detailed insight on transient power supply, dynamic modeling of energy systems onboard ships can be performed. In the last decades, significant effort has been paid by the scientific community to develop numerical models able to predict the time-dependent operating conditions of gas turbines. Schobeiri et al. [19] developed a detailed 1-D model to modularly assess the dynamic behaviour of turbomachinery and combustors. Hou et al. [20] proposed a fast Model Predictive Control (MPC) for gas turbine units aimed at realizing safe and efficient operation of Combined Cycles (CC), whereas Rùa et al. [21] proved that linear MPC is able to implement optimal control sequence for stress monitoring in CC, opposite to nonlinear models. Kim et al. [22] investigated transient performances of aero-engines by means of a performance adaptation approach and found out that turbomachinery map scaling can improve temperature control system. Tsoutsanis et al. [23] defined a novel compressor map tuning method able to improve the high-fidelity of GT models for performance prediction and diagnostics, whereas Hadroug et al. [24] proved that accurate time-dependent results can be similarly achieved by linearization. Wang et al. [25] developed a new physics-based models of hydraulic fuel systems for GTs, which was shown to increase accuracy with respect to transfer function models. Recently, machine learning techniques have been used to build black or gray box model of GT dynamics in the loading and unloading operating conditions [26,27] or for maintenance and prediction purposes [28]. Where steam power plant modeling is concerned, Zhao et al. [29] focused on the lumped volume modeling of steam power plants in nuclear Boiling Water Reactor (BWR), whereas Alobaid et al. [30] developed an Heat Recovery Steam generator (HRSG) model for combined cycle power plants by means of a six equation system solving for two phase flows. Pondini et al. [31] focused on steam turbine control systems, showing that new actuation technologies should be developed in order to meet response capability required by the current power generation sector. Beiron et al. [32] investigated how three different types of flexibility measure impact on Combined Heat and Power (CHP) cycle revenue and underlined how product flexibility on electrical and thermal power supply guarantees the highest cost savings. Mertens et al. [33] assessed the dynamical impact of including a once-through or natural circulation evaporator within a combined cycle HRSG, while Sun et al. [34] found out that a 5–7 % lower steam turbine inlet pressure guarantees higher power production in case of flexible operating conditions for CHP.

Following the investigation presented in Dotto et al. [10], this work aims at demonstrating the benefits provided by COGES plants in terms of efficient energy utilisation onboard a cruise ferry. Specifically, the work is a feasibility study developed according to the GNV shipowner's need of new power plant to be installed onboard La Suprema, able to guarantee high energy efficiency under flexible operating conditions. In order to obtain more detailed results, many GTs have been accounted for and transient operation is also assessed. Dynamic simulation is performed through a MATLAB/Simulink code, whose validation is presented in section 4.1, while off-design and transient behaviours of six commercially available GTs are analysed in section 4.2. Successively, the optimal repowering plant for La Suprema is identified in section 4.3 and its dynamical performances during actual operating conditions are assessed in section 4.4.

2. Calculation methodology

In this work, two main programs have been used to assess different issues dealing with both simulation of COGES dynamic performance and repowering study applied to the cruise-ferry La Suprema. Specifically, to obtain information not available in the technical sheet provided by the manufacturers, the entire thermodynamic performance of commercially available GTs in nominal operating condition has been firstly reconstructed through a two-step optimization procedure. Secondly, a MATLAB/Simulink program has been developed to model the dynamic behaviour of the gas and steam part of the combined power plant, focusing the attention on different control strategies governing GTs. Thirdly, the performances of the overall repowering plant onboard La Suprema have been optimized by a Fortran code [10] in a quasi-static approach, considering different operating conditions for the ship and various prime mover choices installed within the engine room. From this third step, the repowering plant guaranteeing the highest benefits in terms of cogeneration efficiency and operational ship flexibility is identified. Finally, the dynamic performance of the optimal COGES plant is investigated by the MATLAB/Simulink code applied to the actual sailing condition for La Suprema. In the following, the main characteristics of these programs are reported.

2.1. Two-step optimization code to reconstruct GT nominal conditions

A schematic view of the optimizer is shown in Fig. 1. A thermodynamic cycle computation is performed receiving as inputs:

- P: operational parameters known from the manufacturer (β_c, $\dot{m}_c$, $P_{net,R}$, $\eta_{el,GT,R}$, …)
- X: optimization variables, coinciding with η_{TGG}, η_{PT}, β_{TGG}. Their values are not known a priori, hence the objective of the optimization procedure is to find out them.

Then, a two-step optimization process is performed: the first step consists in formulating the problem as a Multi-Objective Genetic Algorithm (MOGA) where many objective functions, defined as the relative errors for P_{net}, η_{el}, T_{ex}, η_{mec} with respect to the corresponding reference values (see e_1, e_2, e_3 and e_4 in Fig. 1a), must be minimized varying X within the constraints C. The reference values are obtained from the manufacturers, whereas constraints consist in energy balances, continuity equation and thermodynamic relations. The second step consists in formulating a single-objective gradient descent algorithm, where a single cost function takes into account all the relative errors for P_{net}, η_{el}, T_{ex} and η_{mec} by means of a weighted sum. In details, the Genetic Algorithm (GA) starts from a certain population (i.e. ensemble of candidate thermodynamic cycles accounting for various combinations of X), then computes each single individual of it, checks the minimization of the objective function and, finally, moves to a successive generation by means of mutation and cross-over. This process repeats until the Pareto front is found out by the MOGA. In Fig. 1b a 2-D Pareto front accounting for relative errors on T_{ex} and P_{net} is reported. Then, a best individual is identified from the Pareto front and is entered as input for the gradient descent optimization algorithm to explore the solution space around it by considering a single objective function. In this way,

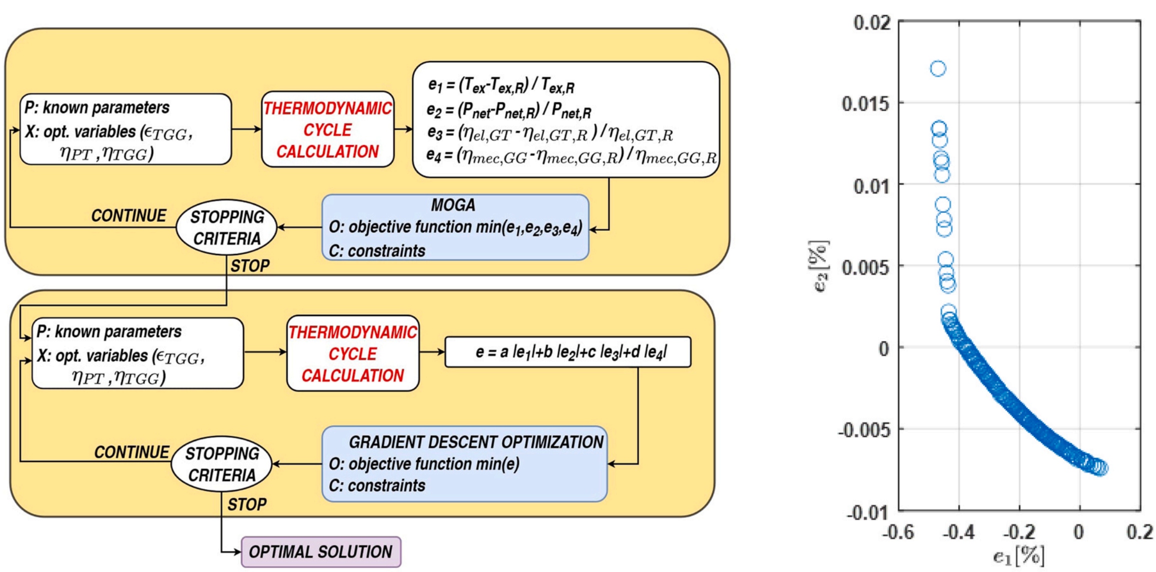

(a) (b)

Fig. 1. Schematic view of the two-step optimization procedure used to reconstruct GT nominal operating conditions (a) and the Pareto front concerning exhaust gas temperature and net power output for the LM2500 GT (b).

the main advantages of both MOGA and single objective optimization are exploited: the MOGA allows the overall exploration of the solution space and, therefore, is reliable in determining the global minimum discarding the local ones. On the other hand, the gradient descent optimization is more accurate than the MOGA in locally exploring the solution space around the global minimum to verify the optimality of the solution. Overall, the double-step optimization procedure reproduced the thermodynamic cycle in nominal condition within 1 % relative error for global performance parameters (i.e. P_{net}, η_{el}, T_{ex} and η_{mec}), for all the six GTs considered in this work.

2.2. MATLAB/Simulink code

The dynamic simulation model of the gas-steam combined power plant built in MATLAB/Simulink consists in a nonlinear lumped volume model described by a set of algebraic and differential equations. Fig. 2 shows the main subsystems of the gas turbine model. Overall, the lumped volume model follows the approach firstly developed in Traverso [35]. The quasi-static response of the component is provided by its performance maps, whereas its time-dependent behaviour is governed by the conservation of mass, momentum and energy as reported in general form in equations (1), (2) and (3), respectively:

$$\frac{\partial}{\partial t}\int_{CV}\rho dV + \int_{CS}\rho\boldsymbol{V}\cdot dA = 0 \tag{1}$$

$$\frac{\partial(mU)}{\partial t} = \frac{\partial}{\partial t}\int_{CV}\rho\boldsymbol{U}dV - \int_{CS}\rho\boldsymbol{U}(\boldsymbol{U}\cdot\boldsymbol{n})dA \tag{2}$$

$$\frac{\partial\tilde{E}}{\partial t} = \int_{CV}\frac{\partial\rho\tilde{e}}{\partial t}dV - \int_{CS}\rho\tilde{e}\boldsymbol{V}\cdot\boldsymbol{n}dA = \dot{q} \tag{3}$$

where ρ indicates density, U the flow velocity, V the control volume, A the surface, m the mass, n the vector locally normal to the control surface, $\tilde{E}$ the total energy and $\tilde{e}$ the total energy per unit of mass. Then, an interconnecting plena approach is used to connect each component to the adjacent ones by means of compatible boundary conditions. To this end, the intermediate volumes V_c and V_t, where the mass and energy conservation equations are solved in time, have been inserted (see Fig. 2). Two main control strategies which are common in CHP plants have been implemented for governing GTs:

- *TIT ≈ const* in order to maximize efficiency of gas turbine engine at part-loads. In the following the acronym TITc is used for this strategy
- *TOT ≈ const* aimed at optimizing the operating condition of the bottoming steam power plant at part-loads. Specifically, a safety and efficient operation is ensured for the HRSG. In the following the acronym TOTc is used for this strategy

From the power generation field, it is well known that the second strategy allows the optimal performance of the overall gas-steam combined cycle [36,37]. Safety controllers for over-temperature and over-speed have been implemented to avoid thermo-mechanical damages during transient operation. Specifically, the threshold beyond which the over-temperature and over-speed controllers take action has been fixed to 105 % and 110 % of the nominal values, respectively. Finally, the following-load service, which is typical of combined power plants, is guaranteed by the fuel feeding PID controller in compliance with the safety operation controllers. Overall, all the controllers act on varying the fuel consumption and the Inlet Guide Vane (IGV) position and are inserted within fuel feeding system and IGV blocks of Fig. 2. In details, as visible in Fig. 2, the IGV block receives as input the N_{GG}, T_{ex} and $T_{i,TGG}$ signals to determine the IGV angle, whereas the fuel feeding system block decides the fuel mass flow rate depending on both net power produced by PT and the inlet temperature to the GG turbine.

On the other hand, Fig. 3 shows the mixed lumped volume-dynamic model developed for the bottoming steam power plant. The turbomachinery components are modeled using a nonlinear lumped volume scheme analogous to that explained above for GT, whereas the heat exchangers are solved by a 2-D dynamic approach. Specifically, a shell-and-tube configuration has been adopted and the corresponding finite difference scheme used for single phase heat exchangers is shown in Fig. 4, where $\dot{q}$ indicates conductive/convective heat fluxes. A staggered grid of nodes is adopted to guarantee a good compromise between accuracy and numerical effort [35]. Overall, the interconnecting protocol between blocks as well as the control strategy for the steam bottoming power plant shown in Fig. 3 have been chosen taking into account the results found by Benato et al. [38]. Specifically, the main feed-water system P1 controls the saturation pressure level within the evaporator drum such as risks of burning the evaporator tubes or flooding portion of the superheater are avoided. The sea water pump P2 is regulated by a PID controller whose target is maintaining constant in time the level of the condensed water. Finally, the PAR block performs the partialization regulation of the ST.

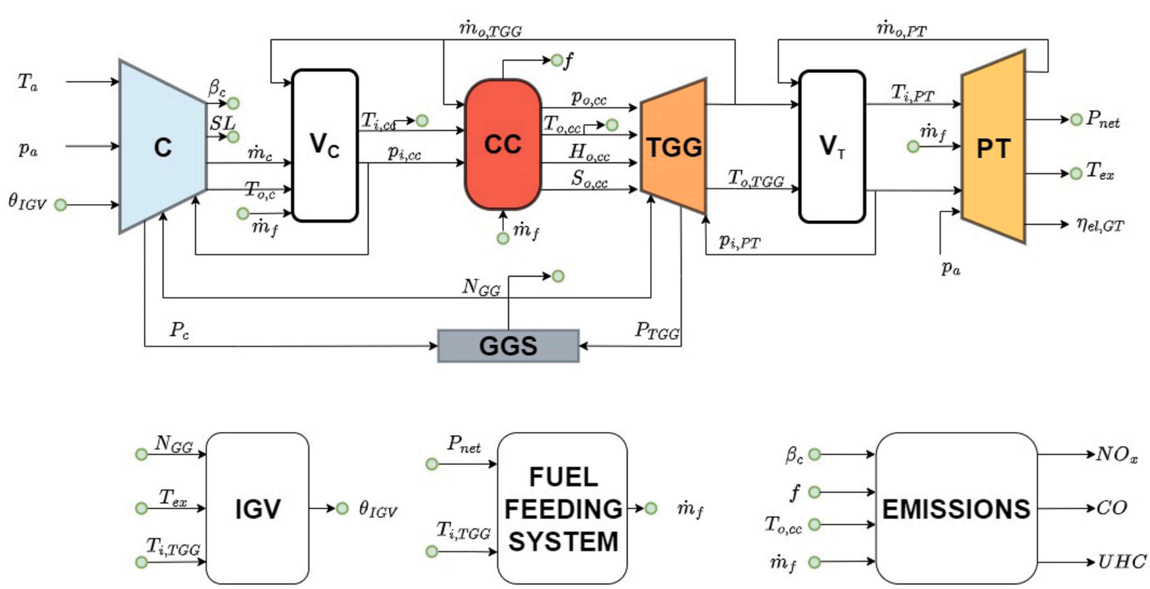

Fig. 2. Simulink block diagram for the GT model.

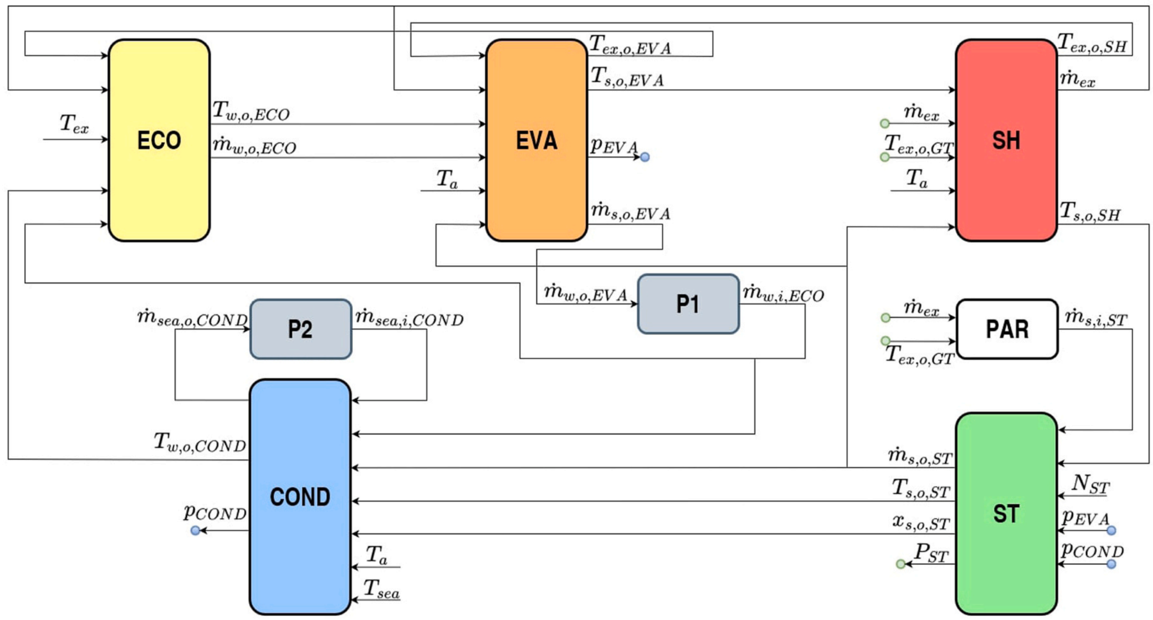

Fig. 3. Simulink block diagram for the bottoming steam power plant model.

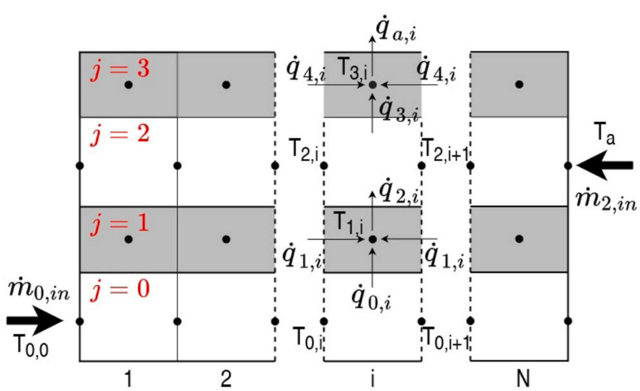

Fig. 4. General finite difference scheme adopted for single-phase heat exchangers within HRSG.

2.3. Fortran code

The Fortran program is able to optimize the working conditions of ship power plants, adopting a steady state modeling approach. Specifically, the optimization of cogeneration efficiency may be performed for various ambient temperature and ship speed operating conditions. The working principle of the Fortran code can be divided into three main steps:

- *COGES plant design and off-design performances:* for each GT to be installed onboard, the Heat Recovery Steam Generator (HRSG) is optimally designed to maximize waste heat recovery from exhaust gas and the overall bottoming steam power plant is set up. In this work, a condensing steam turbine is considered to increase electrical power output. Then, the performances of the overall COGES plant are computed in off-design conditions varying load and ambient temperature.
- *Setting up the objective function:* both electrical or cogeneration efficiency can be considered as objective functions to be maximized. In this work the cogeneration efficiency is maximized.
- *Optimization of power plant installed onboard:* the code determines which prime movers need to be lighted on and at which load to maximize the objective function in each ship operating condition. The optimization process is based on a full-factorial numerical scheme.

More details concerning the Fortran code can be found in Dotto et al. [10].

3. Case Study

The power plant currently installed onboard La Suprema, whose main characteristics are reported in Table 1, was designed for a cruise speed of 28 knots and a maximum speed of 30 knots [10]. The ship propulsion system actually installed onboard consists of two controllable pitch propellers, each driven by two Wartsila 16V46C Diesel engines, delivering 16,800 kW at 500 rpm. Four Wartsila-Vasa 6R32LNE Diesel generators (9.7 MW overall electrical power) satisfy power demand for harbour and manoeuvring operating conditions. However, La Suprema is currently sailing on the Genova-Palermo route at 22 knots, hence its actual power plant works far from the design cruise speed, with negative consequences on efficiency and fuel consumption. Specifically, only two Wartsila 16V46C engines work at part-load to cover propulsion demand, with consequent drawbacks in terms of primary energy savings and operational costs for the shipowners. For these reasons, a repowering study for La Suprema is performed to improve energy efficiency and limit operational expenditure, according to specific requests from the shipowners [10]. Furthermore, the repowering plant needs to guarantee high performances under extremely flexible operating conditions, comprehensive of various GNV routes within the Mediterranean sea, as required by shipowners. Fig. 5 reports the power demand comprehensive of the propulsion and hotel loads on board La Suprema for variable ship speed and season. Specifically, P_o indicates the propulsion demand, whereas $P_{b,w}$ and $P_{b,s}$ are the total brake power for winter and summer seasons, respectively. The power demands required on current GNV Mediterranean routes are highlighted with markers, where GP stands for Genoa-Palermo route, GB for Genoa-Barcelona, NP for Naples-Palermo and NC for Naples-Catania. Furthermore, the thermal power demand onboard La Suprema during

Table 1
La Suprema main characteristics.

Dimension	Value
Length between perpendicular LPP [m]	186.21
Deadweight tonnage DWT [t]	9720
Volume ∇ [m^3]	25733

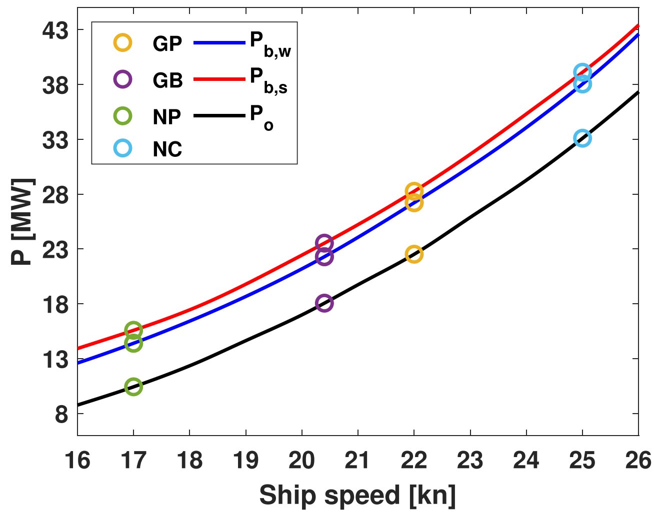

Fig. 5. Hotel and propulsion electrical powers required by La Suprema for summer and winter seasons.

cruise operating condition consists of 900 kg/h and 1050 kg/h steam mass flow rates at 7 bar for summer and winter seasons, respectively. To preserve power plant flexibility and high efficiency in case of different ship operating conditions, performance of candidate repowering plants for La Suprema has been investigated over a wide range of ship speeds (16–26 kn). In this work, the integrated electric power plant schematically depicted in Fig. 6 is investigated. For a generality purpose, reciprocating engine blocks are indiscriminately depicted in Fig. 6 for both large and small size reciprocating engine solutions. Analogously, dots at the electric bar indicate variable number of both prime movers and power users. Overall, two DF reciprocating engines of variable size, three natural gas (NG) engines and a COGES plant are included as prime movers driving variable speed generators. Waste heat is recovered by DF engines to generate steam at 7 bar, whereas no WHR systems are coupled with natural gas engines due to their small size. It must be remarked that NG engines constitute harbour generating set but they are allowed to run also on cruise operating conditions in case they may provide benefits in terms of power plant efficiency [39]. Table 2 reports all the prime movers considered in the repowering study. Specifically, six different GTs, two different dual fuel MAN reciprocating engines and a natural gas Rolls-Royce reciprocating engine for the harbour generating requirements have been considered. As can be seen, in order to accurately design highly-efficient repowering plant for La Suprema, six different GTs dealing with variable size and thermodynamic performances are considered. Indeed, it can be noticed that two GTs (LM2500+ and LM2500 + G4) are characterized by major size, whereas other two GTs (SGT600 and RB211) present intermediate efficiency together with low exhaust gas temperature and mass flow rate. On the other hand, intermediate size and quite large waste heat available for the bottoming steam power plant are related to LM2500 and TITAN250 GTs. Furthermore, differently from 12 V MAN and 9 L MAN, no exhaust gas temperature for the reciprocating engine R-R Bergen C26 L9 is provided, since it deals with no WHR system, owing to its small size.

Furthermore, Table 3 reports the power plant configurations investigated in the present study, with the aim of maximizing cogeneration efficiency over a wide ship speed range. The propulsion plant design procedure proposed by the MAN company [40] has been adopted in selecting all power plant configurations reported in Table 3. Furthermore, it must be underlined how the DF engines dealing with higher P_{net} (12VMAN) have been coupled with large size GTs to supply power demands at intermediate ship speeds (18–21 knots), where GT performances are negatively affected by part-loads and 9LMAN engines result insufficient to cover the power request. Furthermore, both the TITc and TOTc control strategies have been investigated for each GT.

4. Results

4.1. Validation

The validation of MATLAB/Simulink codes has been carried out to verify their reliability in reproducing performances of both GTs and steam power plants. Towards this end, experimental datasets available from the literature have been considered as reference for the comparison.

First, the GT code has been validated considering data for 32 MW LM2500 + G4 gas turbine fed by MDO and currently installed onboard military ships [41]. The Turbine Control System (TCS) determines the fuel mass flow rate depending on the gas generator required speed, which is proportional to power. Furthermore, TCS ensures safety operating conditions in terms of over-speed of power turbine and over-temperature of the gas flow exiting the gas generator turbine. Table 4 reports the errors obtained by comparing experimental data with numerical results provided by the optimization and MATLAB/Simulink codes, whose architecture and boundary conditions were set to reproduce the reference gas turbine. Results referring to 25 %, 50 %, 75 % and 100 % working load conditions are reported in relative form, for industrial confidentiality reasons. Specifically, relative errors are defined as $(V_{exp} - V_{num})/V_{exp}$, where V_{exp} and V_{num} represent the experimental and numerical values of each parameter reported in Table 4, respectively. The parameters available for validation consist of electrical power generated by GT, $P_{el,GT}$, and its corresponding electrical efficiency, $\eta_{el,GT}$, the rotational speed of gas generator shaft N_{GG} and power turbine N_{PT}, the fuel mass flow rate $\dot{m}_f$ injected within the combustion chamber, pressure and temperature of the air flow entering the combustion chamber (i.e. $p_{i,cc}$ and $T_{i,cc}$, respectively), pressure $p_{o,TGG}$ and temperature $T_{o,TGG}$ of the flow exiting the gas generator turbine. As can be seen, relative errors do not exceed 2 % for all the parameters experimentally available from the manufacturer, over the entire load range tested. Therefore, the reliability and accuracy of both two-step optimization and MATLAB/Simulink codes in reproducing the thermodynamic working conditions of GTs are well established.

Where the steam power plant included within COGES configuration is concerned, validation has been carried out considering field data referring to the natural gas fed combined cycle located at the Oseberg Field Center, in the North Sea [42]. The reference power plant consists of two GE LM2500+ gas turbines, which are coupled with a one pressure level heat recovery steam generator (HRSG) producing steam at 24 bar. Then, steam feeds a condensing ST and expands up to 0.05 bar to generate electrical power. The flow exiting the steam

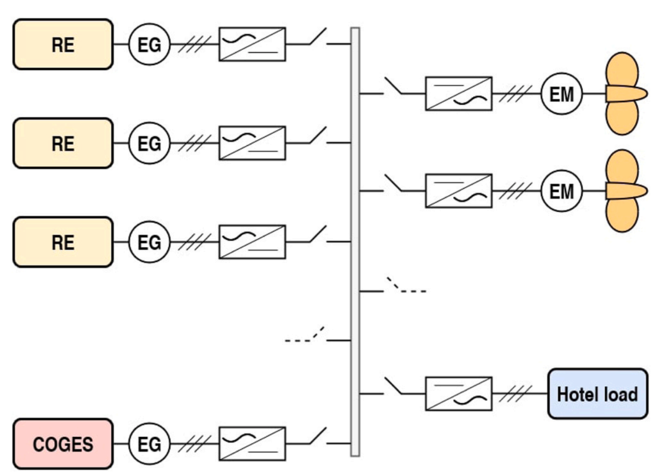

Fig. 6. Schematic view of the integrated COGES-reciprocating engine power plant investigated. RE indicates reciprocating engines (both dual-fuel and natural gas engines), EG stands for electrical generator, EM means electrical motors.

Table 2
Prime mover main characteristics.

GT	P_{net} [MW]	$\eta_{el,GT}$ [%]	T_{ex} [°C]
LM2500	25.06	37	566
TITAN250	21.75	39	465
SGT600	25.30	35	543
RB211	26.03	36	488
LM2500+	30.20	39	518
LM2500+G4	36.98	40	549
12 V MAN 51/60	11.23	45.5	309
9 L MAN 51/60	8.42	45.5	309
R-R Bergen C26 L9	2.33	45	–

Table 3
Propulsion system configurations.

GT	12VMAN51/60	9LMAN51/60	R-R C26L9
LM2500		XX	XXX
TITAN250		XX	XXX
RB211		XX	XXX
SGT600		XX	XXX
LM2500+	X	X	XXX
LM2500+G4	XX		XXX

Table 4
Relative errors obtained comparing experimental data and numerical results for LM2500 +G4 gas turbine at 25 %, 50 %, 75 % and 100 % load operating conditions.

Parameters	100 %	75 %	50 %	25 %
$P_{el,GT}$	0.06	0.07	0.06	0.05
$\eta_{el,GT}$	0.52	1.84	1.47	0.70
N_{GG}	1.21	−0.03	−0.23	0.26
N_{PT}	0.00	0.00	0.00	0.00
$\dot{m}_f$	−0.53	−1.85	−1.48	−0.66
$p_{i,cc}$	0.15	0.55	1.03	1.62
$T_{i,cc}$	0.19	−0.26	−0.25	0.55
$p_{o,TGG}$	−1.46	−0.85	−0.08	1.03
$T_{o,TGG}$	1.40	−0.03	−0.21	0.25

turbine is cooled by sea water at 8°C within the condenser module (T_a=9°C). Overall, ST is controlled by means of both partialization and lamination modes. Therefore, in order to validate the code concerning the steam bottoming power plant, the architecture reported in Nord and Montañés [42] as well as its initial and boundary conditions (e.g., exhaust mass flow rates and temperatures from GTs) have been reproduced, hence guaranteeing comparability with the reference work. Specifically, comparison between the thermodynamic parameters reported in Nord and Montañés [42] and numerical results obtained from the code concerning steam power plant is carried out in Table 5. Specifically, relative errors defined as $(V_{exp} - V_{num})/V_{exp}$ are shown for 20 %, 40 %, 60 %, 80 % and 100 % load operating conditions of LM2500+ GTs, as reported by Nord and Montañés [42]. Validation accounts for data concerning the ST inlet pressure $p_{i,ST}$ and temperature $T_{i,ST}$, the steam mass flow rate $\dot{m}_s$ evolving within ST, the discharge pressure at condenser p_{COND}, the rotational speed of ST N_{ST}, the electrical power delivered by steam turbine $P_{el,ST}$, the sea water mass flow rate $\dot{m}_{sea,COND}$ required for condensing purposes, the exhaust gas temperature T_{ex} and mass flow rate $\dot{m}_{ex}$ from the LM2500+ gas turbine. As can be seen, numerical results obtained from the code show good agreement with the Oseberg Field Center data reported by Nord and Montañés [42]. Specifically, all the relative errors do not exceed 2 % over the entire load range under investigation. Thus, the MATLAB/Simulink code shown in Fig. 3 is proved to reliably model the design and off-design performances of the bottoming steam power plant in combined cycle configuration.

4.2. Dynamic results from GT model for variable control strategy

In this section, the dynamic behaviour of GTs provided by the MATLAB/Simulink model is investigated, focusing on the time-dependent trace concerning the most relevant operating parameters. For the sake of conciseness, only the results from the LM2500 gas turbines are presented, since other GTs show performance qualitatively analogous, despite different in values. In the following, results are reported distinguishing 3 different operating principles for the GT: in addition to the TITc and TOTc strategies introduced in section 2.2, the time-dependent results obtained excluding the Variable Inlet Guide Vane (VIGV) actuation is considered as reference and indicated by the acronym Fc.

Fig. 7 reports on the compressor map the equilibrium running lines, i.e. the locus of equilibrium states for the machine, obtained by imposing to the gas turbine model a power demand ranging from 20 % to 100 % of the GT load. Operational points corresponding to 20 %, 40 %, 60 %, 80 % and 100 % loads are reported with different shapes and colors. In the same figure, also the equilibrium running line available in the literature for the LM2500 is reported for comparison (dashed black line) [43]. The iso-contour lines of N_{gg} and η_c are reported in purple and blue, respectively, whereas the surge line is pictured by dash-dot line. It can be clearly seen how all the 3 equilibrium running lines are positioned far away from the surge line, thus no compressor stall is surveyed and safety operation is preserved. Specifically, defining the surge limit as [43]:

$$SL = \frac{p_{surge} - p(t)}{p(t)} \quad with\ \dot{m}_c = const \tag{4}$$

all the 3 equilibrium running lines deal with $SL \geq 0.22$. Furthermore, comparing the reference equilibrium line (dashed black curve) provided by Klapproth et al. [43] with the numerical results, a good agreement arises over the entire load range. As visible from Fig. 7a the equilibrium point corresponding to the minimum load imposed in the start up procedure (20 %) deals with different positions when the VIGV actuation is enabled. Indeed, green and light blue lines clearly extend at lower mass flows in comparison with the blue curve (i.e. no VIGV control). This is mainly due to the role played by the VIGV in reducing the mass flow passing through the compressor inlet vanes by modifying their stagger angle [44–46]. The influence exerted by the VIGV angle on the compressor characteristic map in terms of β_c, $\dot{m}_c$ and η_c has been desumed from previous works applying a scaling approach [47–49]. Differences between the green and light blue curves reported in Fig. 7a directly depend on the VIGV actuation law adopted to govern the GT and reported in Fig. 7b. Indeed, starting in full-opened condition at 100 % load, VIGV reaches its maximum closure at 30–50 % load depending on the control strategy, thus it can not regulate the mass flow to keep TIT or TOT constant for further reduced loads. For this reason the green and light blue curves nearly coincide for $\dot{m}_c \leq 40 kg/s$.

Table 5
Relative errors obtained comparing reference datasets from the Oseberg Field Center combined cycle [42] with simulation results for the bottoming steam power plant shown in Fig. 3. Comparison has been carried out at 20 %, 40 %, 60 %, 80 % and 100 % GT load operating conditions.

Parameters	100 %	80 %	60 %	40 %	20 %
$p_{i,ST}$	0.00	+0.06	+0.06	+0.15	+0.15
$T_{i,ST}$	+1.87	1.25	+1.05	+0.83	−0.26
$\dot{m}_{s,i,ST}$	−0.10	−0.53	−0.30	−0.31	−0.04
p_{COND}	−0.3	−0.64	−0.98	−1.32	−1.62
N_{ST}	0.00	0.00	0.00	0.00	0.00
$P_{el,ST}$	−0.09	+0.52	+1.31	+0.88	+1.04
$\dot{m}_{sea,COND}$	−0.98	+0.13	−1.91	−0.08	+1.33
T_{ex}	−1.50	−1.30	−1.25	0.00	−0.01
$\dot{m}_{ex}$	−0.01	+0.07	−0.02	+0.07	+0.01

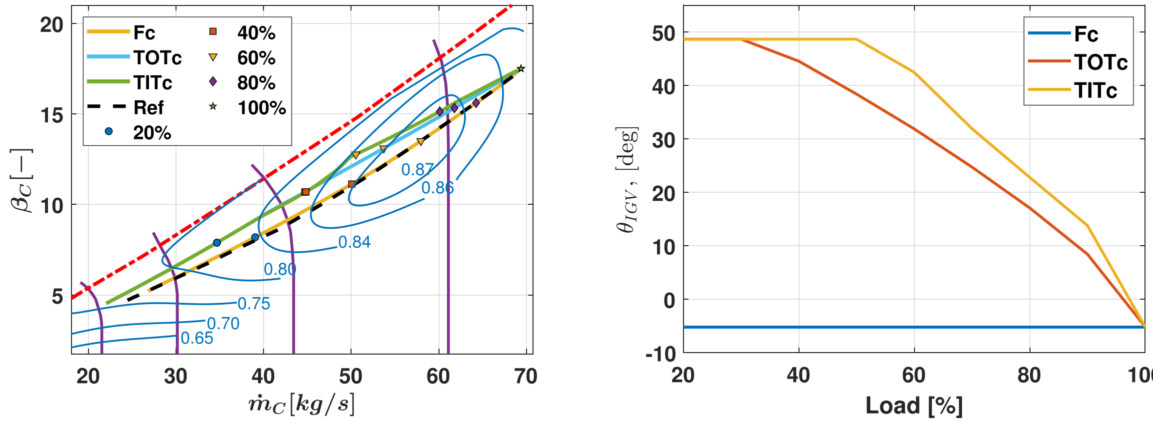

(a) (b)

Fig. 7. Equilibrium running lines for TITc, TOTc and Fc control strategies on the compressor maps (a) together with the corresponding VIGV actuation laws (b).

In order to provide a more detailed view of thermodynamic operating conditions involved with Fc, TITc and TOTc control strategies, Fig. 8 reports the time-dependent results concerning P_{net}, *TIT*, T_{ex} and N_{gg}, together with the start-up/switch-off load ramps (i.e. power demand from electric generators) provided as input. The start-up load ramp consists in varying the electric power requested from 0 to the nominal power delivered by gas turbine in 50 s, and viceversa for the switch-off ramp. Fig. 8 shows a nearly symmetric behaviour of all the thermodynamic parameters for an accelerating and decelerating ramp. Focusing on the N_{gg} plot along the switch-off ramp, over-speed condition for the TITc strategy occurs around $t = 10-23s$ (load $\approx$ 60 − 70 %), where a N_{gg} plateaux induced by the over-speed PID controller is clearly visible. Indeed, comparing the *TIT* and T_{ex} time dependent curves for all the three control strategies, the fuel flow rate decrease imposed at partial-loads implies a reduction in the *TIT* in case of no actuation on the VIGV (see the blue curve). On the other hand, VIGV is closed in TITc and TOTc strategies to keep reference temperatures constant, so that acceleration of the GG shaft is induced [50]. Since the VIGV closing step required by TITc for a certain load variation is higher than that needed by TOTc (see Fig. 7b), the N_{gg} increase is stronger for the yellow curve, which exceeds the over-speed limit (i.e. 110 % of the nominal N_{gg}). When the required load further reduces, the over-speed is damped by the simultaneous decrease of $\dot{m}_f$ and VIGV opening angle, hence the over-speed control stops working. Analogous comments can be made for the accelerating ramp. Finally, to better understand the load range where TITc and TOTc carry out their tasks successfully, the *TIT* and *TOT* variations in function of the load are reported in Fig. 9 referring to these two control strategies. As can be clearly seen, the TOTc strategy succeeds in keeping constant T_{ex} up to approximately 30 % of the load, hence guaranteeing reduced off-design operating conditions for steam power plant in combined cycle configuration. On the other hand, the TITc strategy manages to keep the turbine inlet

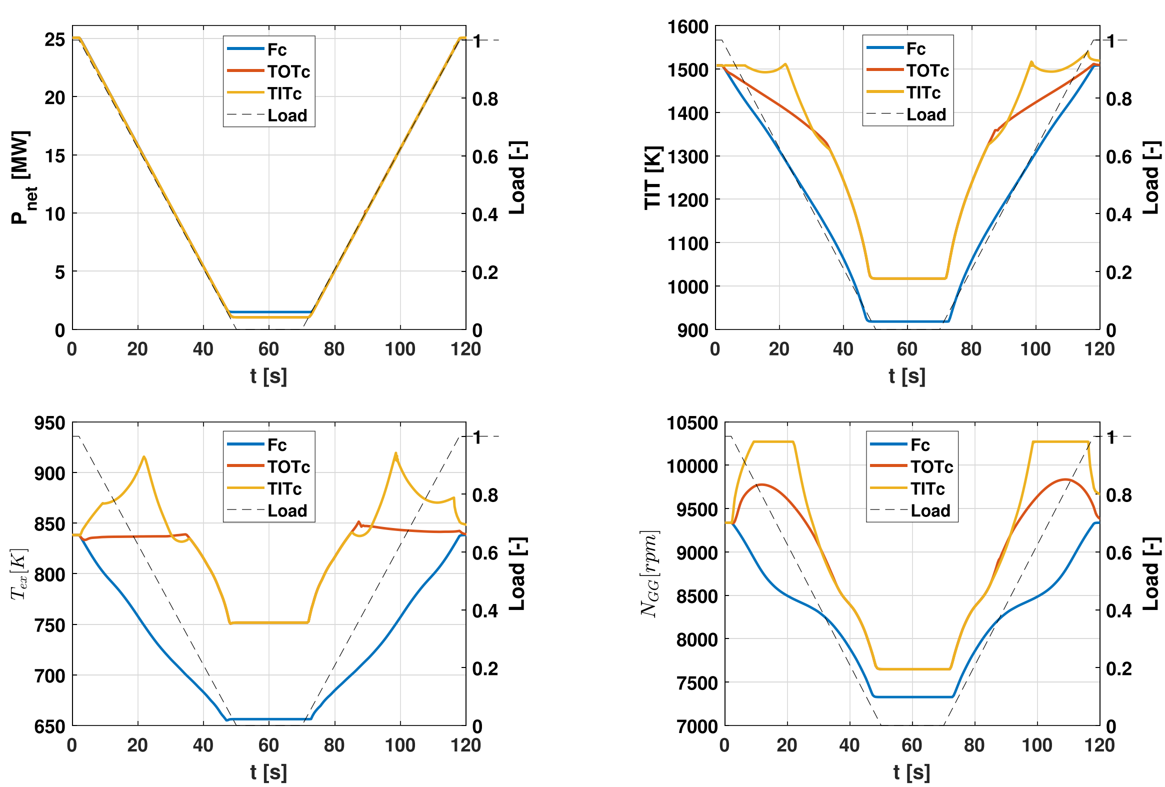

Fig. 8. Time-dependent behaviour concerning the main GT thermodynamic parameters for TITc, TOTc and Fc control strategies: net power (a), TIT (b), T_{ex} (c) and N_{gg} (d).

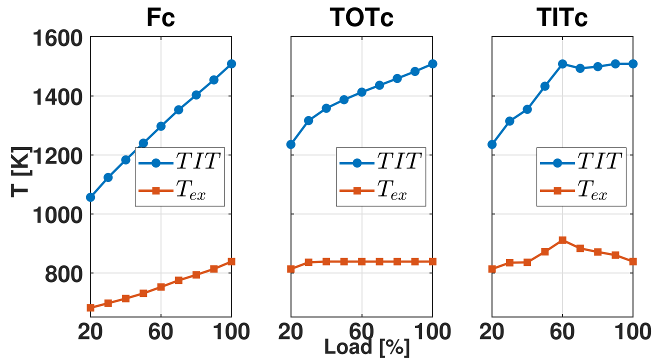

Fig. 9. Variability of T_{ex} and TIT in terms of load for (from left to right) Fc, TOTc and TITc control strategies.

temperature constant up to 70 % of the load, where the over-speed control takes action reducing *TIT*, as shown above. However, deviations from the reference *TIT* are particularly reduced up to the 60 % load (relative error < 2 %). Overall, these results fairly agree with the literature [48]. Finally, it must be underlined that the dynamic models concerning the other 5 different GTs show results qualitatively analogous to those presented above for the LM2500 gas turbine, thus they are not presented here for sake of conciseness.

4.3. Repowering plant optimization for the cruise-ferry La Suprema

In this section, comparison on efficiency parameters is assessed for all the 6 power plant configurations summarized in Table 3. Specifically, results concerning the cogeneration efficiency, defined by eq. (5), are reported:

$$\eta_g = \frac{\sum_{i=1}^{N_{eng}} P_{el,i} + P_{th,i}}{\sum_{i=1}^{N_{eng}} \dot{m}_{f,i} LHV_{NG} + \sum_{j=1}^{N_{DF}} \dot{m}_{f,j} LHV_{MDO}} \tag{5}$$

where N_{eng} is the active engine number, N_{DF} the number of DF reciprocating engines, LHV_{NG} the lower heating value of LNG, LHV_{MDO} the lower heating value of MDO used in reciprocating engine pilot flame, $P_{el,i}$ and $P_{th,i}$ the useful electrical and thermal power delivered by the i-th engine, $\dot{m}_{f,i}$ the LNG mass flow rate used by the i-th engine, $\dot{m}_{f,j}$ the MDO mass flow rate used by the j-th DF reciprocating engine. In order to design a power plant which guarantees high energy savings in flexible operating conditions for the cruise-ferry La Suprema, performances are assessed for two seasons (winter and summer) and for 11 ship speeds. Both TITc and TOTc schedules are considered in the analysis, so that the best governing strategy for marine GT included within a COGES plant is identified.

Fig. 10 shows the cogeneration efficiency results obtained from all the 6 different power plants in case TOTc strategy is implemented. The left and right plots refer to the winter and summer seasons, respectively, whereas the tabular legend contains engine load information in percentage of maximum continuous rating for the entire ship speed range 16–26 knots. The COGES plants are identified by the GT module, whereas DF1 and DF2 refer to dual-fuel engines (12VMAN, 9LMAN), and B1, B2 and B3 indicate R-R Bergen C26 L9 engines. From Fig. 10, the cogeneration efficiency curves obtained from different plants appear characterized by three distinct operating regions, in both winter and summer seasons.

Firstly, the plotted curves are nearly unaffected by the installed COGES plant in the low ship speed range (i.e. ≈ 16–19 knots): small differences arise locally between few curves (e.g. see the purple and light blue curves at 17–18 knots), whereas other curves coincide in a certain ship speed range (e.g. see the purple and red curves for 16–18 knots). The cogeneration efficiency curves approximately coincide at low ship speeds, since only reciprocating (DF or natural gas) engines are turned on by the Fortran code to maximize η_g, as the tabular legend shows. Indeed, 12VMAN, 9LMAN and R-R Bergen C26 L9 reciprocating engines are able to cover the propulsion and hotel loads in the low ship speed range. In case reciprocating engines of the same type are installed and turned on in two distinct machine rooms, the η_g-curves corresponding to these two power plant configurations collapse at the corresponding ship speed. On the contrary, in case all the turned on reciprocating engines are distinct, then the η_g-curves do not coincide. In the latter case, weak variations in η_g are surveyed, since all the reciprocating engines (DF and natural gas) present nearly the same maximum efficiency. Specifically, small-size reciprocating engines can operate at higher loads, i.e. higher efficiency, in comparison to those characterized by larger size, thus their inclusion within the power plant typically reveals to improve energy savings (e.g., see the light blue and purple curves at 17–18 knots). Secondly, the tabular legend clearly indicates that in the central ship speed range (i.e. ≈ 19–23 knots) the propulsion and hotel power demands onboard are covered by COGES plants, since they deliver the requested power with energy saving benefits in comparison with reciprocating engines.

Overall, the load distribution over the entire ship speed range summarized by the tabular legend clearly derives from prime mover size, energy efficiency and performance decay due to partial-loads. Reciprocating engines weakly suffer from partial-loads and, due to their small size in comparison to COGES plants, they can operate at high loads (i.e. high efficiency) even for low ship speeds. In the ship speed range centered around 22 knots, all the COGES plants are able to deliver the requested power more efficiently than reciprocating engines, though the amount of the energy savings benefits depends on the GT the COGES plant is based on. Focusing on the comparison between the 6

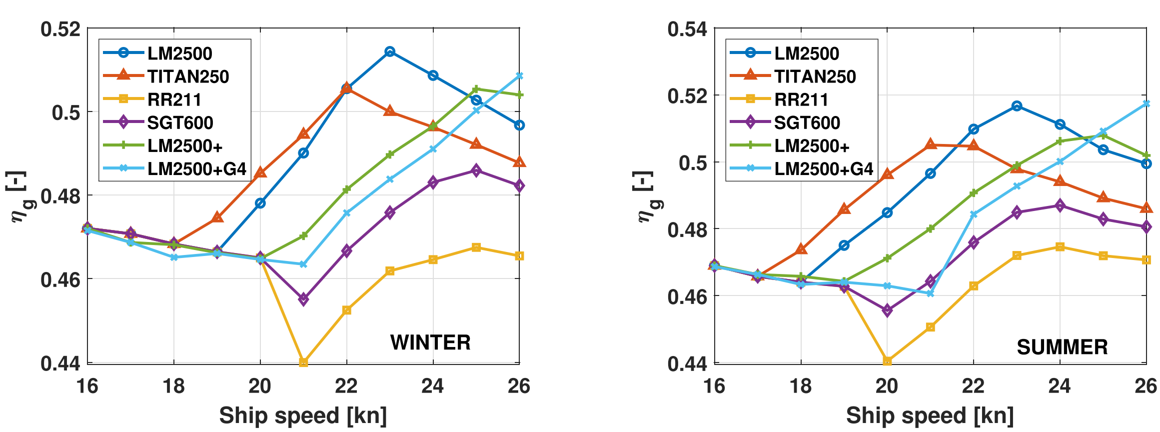

Fig. 10. Cogeneration efficiency considering TOTc control strategy: winter (left) and summer (right) season. The corresponding engine loads are reported in the supplementary materials.

different COGES plants, Fig. 10 clearly shows how the COGES plants based on LM2500 and TITAN250 guarantee the highest performance in the middle-high ship speed range. On the other hand, the COGES plants based on SGT-600 and RB211 provide 1–2 % lower η_g for ship speeds ≥ 20 knots. Indeed, SGT-600 and RB211 deliver nearly the same P_{net} of LM2500 and TITAN250, but with lower η_{el}. Furthermore, their T_{ex} and mass flow rate are lower than those available from LM2500 and TITAN250, hence their bottoming steam power plants can not compensate the reduction in GT efficiency. On the other hand, COGES plants based on LM2500 + and LM2500 + G4 present high cogeneration efficiencies in a limited, high ship speed range. Specifically, they may provide η_g-benefits at 25–26 knots in comparison to LM2500 and TITAN250, though their large size does not allow to efficiently exploit their potential. Indeed, comparing all the curves in Fig. 10, it must be observed that the LM2500 + and LM2500 + G4 curves are shifted towards high ship speeds, thus higher efficiencies may be probably achieved beyond 26 knots.

On the other hand, the cogeneration efficiency results obtained for all the 6 different repowering plants governed by TITc strategy are reported in Fig. 11. As it was for Fig. 10, the left and right plots refer to the winter and summer seasons, respectively, whereas the engine load information is summarized in the tabular legend adopting the same convention for prime mover acronyms. Analogously to what commented out for the TOTc strategy, all the η_g curves appear characterized by three distinct behaviours, depending on the ship speed range, in both winter and summer seasons. The tabular legend clearly confirms that reciprocating engines are turned on in the low ship speed range, whereas COGES plants operate in the middle-high ship speed range, eventually helped by small size reciprocating engines in delivering the propulsion and hotel power requested onboard. Furthermore, comparison between COGES plants confirms that SGT-600 and RB211 appear inadequate when included in a combined gas-steam power cycle, whereas LM2500 + and LM2500 + G4 can not exploit their potential due to their large size. Comparing Figs. 10 and 11, it may be noticed how the η_g is not affected by the GT control strategy in the low ship speed range, and strategies show comparable values when the COGES plants are turned on. However, TITc strategy provides lower cogeneration efficiencies over the entire middle-high ship speed range, especially around the maximum of the efficiency curves (e.g. see the curve concerning COGES based on LM2500 at 24 knots). Indeed, TITc strategy aims at maximizing the electrical efficiency of GT, though it provides reduced exhaust gas temperature and mass flow rate to the bottoming steam power plant, hence resulting in an efficiency reduction for the overall combined cycle. Differently from TITc, TOTc strategy targets the maximization of the energy efficiency provided by the entire COGES plant by dampening the off-design conditions experienced by the steam power plant. However, the bottoming steam power plant is optimally designed from the Fortran code [10], hence this reduces differences between the efficiencies gained by two alternative control strategies (≈ 1 % on η_g). Overall, this result agrees with the terrestrial power plant know-how, where the TOTc strategy applied to combined cycles offers benefits in terms of both energy efficiency and HRSG maintenance. Finally, comparison between COGES plants based on TITAN250 and LM2500 for both TITc and TOTc strategies shows that COGES including TITAN250 leads to significantly higher cogeneration efficiency in a short ship speed range (19–21 knots). Conversely, COGES based on LM2500 offers high performance over a wider ship speed range (19–24 knots). Therefore, the repowering plant based on LM2500, among those investigated, is identified as the optimal one to be installed onboard La Suprema for a flexibility purpose.

In Table 6, the time-mean performance obtained for the LM2500 COGES plant concerning the current sailing ship speed (i.e. 22 knots) are summarised for the sake of clearness.

Table 6
Time-mean results for the Genoa-Palermo route operating conditions.

Results	Summer	Winter
$P_{el,COGES}$	28.26 MW	27.22 MW
$\eta_{el,COGES}$	50.06 %	49.46 %
$\eta_{g,COGES}$	50.98 %	50.54 %

4.4. Dynamic simulation of optimal repowering plant for the current operating condition of the cruise-ferry La Suprema

In this section, the dynamic simulation of the current cruise operating condition for the ship La Suprema is performed. From the previous section, the configuration including the COGES based on the LM2500 GT has been selected. Therefore, the dynamic performance of this repowering plant is investigated in this section. The shape of the time-dependet power demand for a typical cruise condition was derived from Baldi et al. [51]. Since the current cruise speed for La Suprema (i.e. 22 knots) belongs to the ship speed range where only the COGES plant is turned on to maximize cogeneration efficiency, no dynamic model for the reciprocating engines is needed. Furthermore, the previous section showed that cogeneration efficiency maximization is achieved by the TOTc control strategy, thus this governing method is adopted here for the GT engine.

Fig. 12a shows the time-dependent results for the net power output delivered by the COGES plant (continuous line) and the corresponding onboard demand (dashed lines). In particular, the electric power demand has been computed considering a sailing ship speed equal to 22 kn in calm sea over the entire route, whereas time-varying hotel load

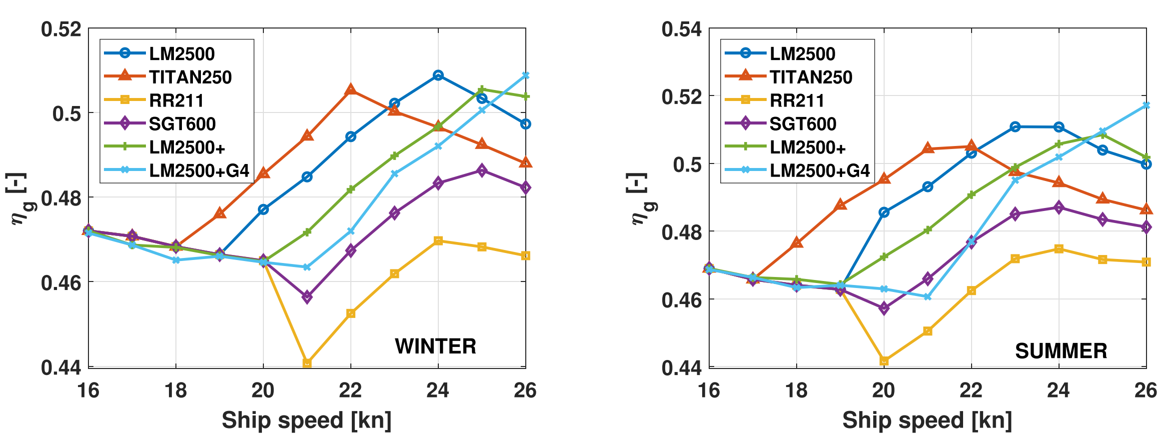

Fig. 11. Cogeneration efficiency considering TITc control strategy: winter (left) and summer (right) season. The corresponding engine loads are reported in the supplementary materials.

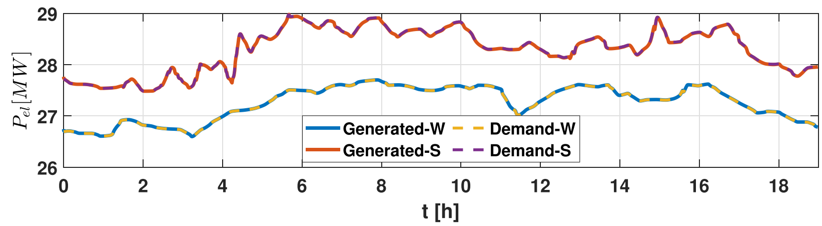

(a)

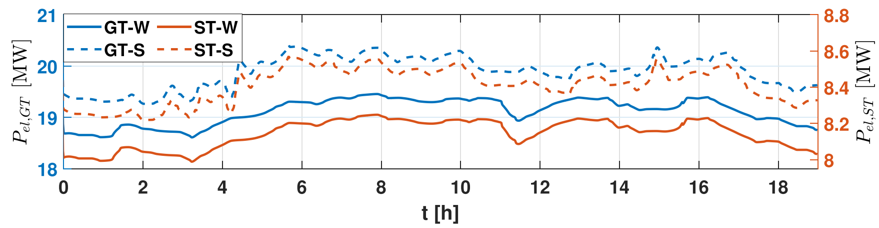

(b)

Fig. 12. Time-dependent performance for the cruise operating condition of the ship GNV La Suprema, for winter and summer seasons.

is accounted for. Winter and summer curves are shown in yellow and purple for the power demand, and in blue and red, respectively, for the delivered power. The time domain extension coincides with the duration of the cruise condition on the Genova-Palermo route (i.e. 19 h), thus a real-time simulation is performed. Interestingly, it can be observed how the COGES plant guarantees a quick-response load-following service, since the requested power onboard is closely followed over all the 19 h. This is in agreement with what occurs in the heavy-duty power plants, where combined cycle ability to perform I, II and III frequency reservoir is well-established. Furthermore, Fig. 12b splits the COGES power output into the components of gas turbine (blue curves) and steam turbine (red curves). Red and blue curves refer to the right-hand-side and left-hand-side axes, respectively, whereas summer and winter seasons are identified by dashed and continuous lines, respectively. It can be observed how the net power produced by the topping and bottoming power plants presents a time-dependency resembling that of the required power. The power available from the gas turbine is nearly twice that delivered by the steam turbine, since small-size GTs are considered in the marine sector, thus limiting the power delivered by the ST with respect to the terrestrial combined cycle field [36,52–54]. Specifically, the power produced by the steam bottoming cycle is in agreement with commercially available ST installed onboard ships [55–57].

To provide a more detailed view on the transient time-dependent analysis for the COGES plant, Fig. 13 shows the thermodynamic signals which are most important from a dynamic perspective. Blue and red

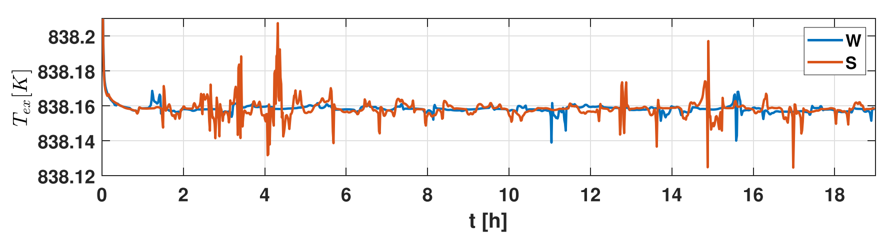

(a)

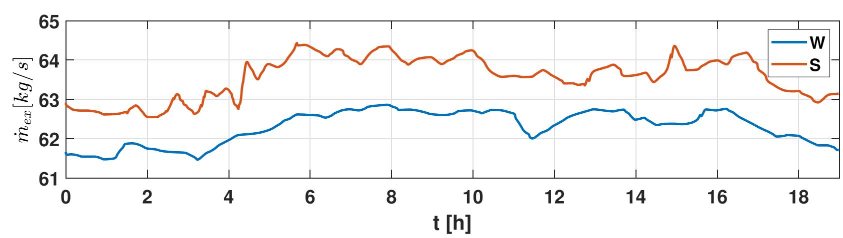

(b)

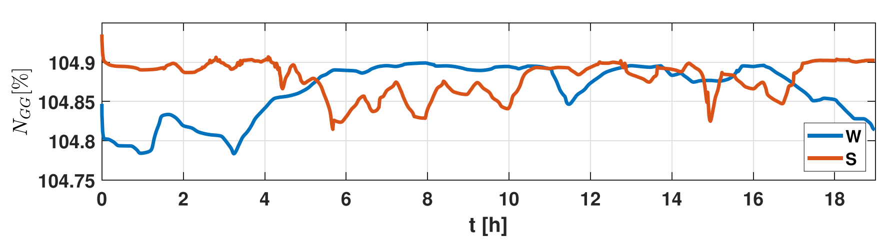

(c)

Fig. 13. Time-dependent results concerning the exhaust gas temperature T_{ex} (a), the exhaust mass flow rate $\dot{m}_{ex}$ (b) and the gas generator rotational speed N_{gg} (c) during the cruise operating condition of the ship La Suprema, for winter (W) and summer (S) seasons.

signals correspond to winter and summer season, respectively. In particular, Fig. 13a shows that the exhaust gas temperature exiting the LM2500 GT remains nearly constant, except for very weak fluctuations induced by the time response of the PID controller in keeping TOT fixed at its nominal value. On the other hand, Fig. 13b shows that the exhaust mass flow rate at the gas turbine outlet section increases when more power is instantaneously requested onboard. The combined effect of TOT and $\dot{m}_{ex}$ motivates the increase in power delivered by the steam turbine for transient growth of requested power onboard ship, since more thermal energy is captured by the HRSG (see Fig. 12b). Where N_{gg} is concerned (Fig. 13c), the rotational speed of the GG shaft exceeds its nominal value for nearly 4 %, in both winter and summer operating conditions. As commented out in section 4.2, this exceeding mainly derives from the closing command actuated on the VIGV and aimed at keeping TOT fixed at its nominal value, when the GT moves from the 100 % load condition. Thus, the gas generator accelerates for a 4–5 % with respect to the nominal rotational speed, since at 22 knots the LM2500 GT is working at partial-load. Focusing on the winter season, N_{gg} follows the time-dependent profile of requested power, whereas in summer N_{gg} experiences a local reduction for power demand around 19–20 MW. This manly derives from the change in dependency experienced by $N_{gg} = f(load)$ and shown by the red curve in Fig. 8: by reducing the required power, N_{gg} temporarily increases (without reaching the over-speed limit) and then, when the load continues to fall down, N_{gg} decreases. Since the maximum of the N_{gg} curve for the TOTc strategy applied to the LM2500 GT occurs around 19–20 MW (see the red curve in Fig. 8), this inversion of proportionality between load and N_{gg} visible in Fig. 13c for requested power around 19–20 MW appears clearly motivated.

5. Conclusions

In the present work, a flexible and modular tool has been developed for the dynamic simulation of COmbined Gas Electric and Steam (COGES) power plants for the marine Liquefied Natural Gas (LNG) propulsion field. Validation of both GT and steam power plant codes has been carried out considering field data present in the literature. Results from all the three successive steps the tool consists in have been presented and analysed. Particularly, a novel two-steps optimization algorithm has been introduced to solve for all the thermodynamic parameters concerning the nominal operating conditions of 6 different commercially available GTs. Overall, the thermodynamic cycles have been solved within 1 % relative error, focusing on global performance parameters provided by manufacturers (i.e. P_{net}, η_{el}, T_{ex}, η_{mec}). In section 4.2, a gas turbine dynamic model for the simulation of off-design and transient operating conditions has been set-up and insight in the physical-based time response of the main thermodynamic parameters is provided. Then, the equilibrium states from the GT dynamic model have been successfully used as input to address a repowering study for the cruise-ferry La Suprema. Specifically, six integrated COGES-reciprocating engines power plants, based on different prime movers, have been investigated in a cogeneration efficiency optimization study. From the optimization procedure, the potential of COGES for the marine field was clearly revealed. In the middle-high ship speed range (19–26 knots), all the 6 COGES plant considered were able to deliver the requested propulsion and hotel power onboard more efficiently than reciprocating engines, providing a 1–5 % higher cogeneration efficiency, depending on the GT the COGES is based on. From section 4.3, two GTs dealing with lower η_{el} and reduced thermal power in the exhaust gas (SGT600 and RB211) revealed low performance, even when coupled to a bottoming steam power plant in a COGES configuration, with 2–3 % efficiency reduction as compared with other COGES plants. The COGES plants dealing with large-size GTs (LM2500+ and LM2500+G4) provided higher cogeneration efficiency at few high ship speeds (25–26 knots), hence their potential can not be effectively exploited onboard La Suprema. The COGES plants based on LM2500 and TITAN250 developed the highest efficiencies (with a maximum of 51 %) over the middle-high ship speed range. Despite the plant including TITAN250 offered higher energy savings benefits on a short ship speed range, the COGES based on LM2500 guaranteed high cogeneration efficiency in a broader operating range, hence it revealed, among those tested, the best combined gas-steam plant to be installed onboard La Suprema for a flexible purpose. Finally, the dynamic and transient simulation of the current ship operating conditions for COGES plant based on the LM2500 GT governed by the TOT constant control strategy confirmed high performances of COGES plant and showed the reliability of the model in reproducing physical-based dynamics. As follow-up work, the flexibility of the codes may be improved to consider even more complex power plant architectures.

Declaration of Competing Interest

The authors declare that they have no known competing financial interests or personal relationships that could have appeared to influence the work reported in this paper.

Acknowledgment

The authors would like to thank Eng. Antonio Campagnuolo and Mr. Marco Fasciolo of the GNV technical office placed in Genoa for supplying data and requirements of La Suprema.

Appendix A. Supporting information

Supplementary data associated with this article can be found in the online version at doi:10.1016/j.nxener.2023.100020.

References

[1] IMO, Report of the marine environment protection committee (MEPC) on its fifty-seventh session 57th session (2008).
[2] IMO, International convention for the prevention of pollution from ships (MARPOL) Annex VI (2011).
[3] P. Balcombe, J. Brierley, C. Lewis, L. Skatvedt, A. Speirs, J. Hawkes, I. Staffell, How to decarbonise international shipping: options for fuels, technologies and policies, Energy Convers. Manag. 182 (2019) 72–88.
[4] S. Horvath, M. Fasihi, C. Breyer, Techno-economic analysis of a decarbonized shipping sector: technology suggestions for a fleet in 2030 and 2040, Energy Convers. Manag. 164 (2018) 230–241.
[5] N. Trivyza, A. Rentizelas, G. Theotokatos, A novel multi-objective decision support method for ship energy systems synthesis to enhance sustainability, Energy Convers. Manag. 168 (2018) 128–149.
[6] M. Altosole, U. Campora, S. Savio, Improvements of the ship energy efficiency by a steam powered turbogenerator in LNG propulsion applications, IEEE (2018) 449–455.
[7] G. Benvenuto, A. Trucco, U. Campora, Optimization of waste heat recovery from the exhaust gas of marine diesel engines, J. Eng. Marit. Environ. 230 (1) (2014) 83–94.
[8] A. Meana-Fernández, B. Peris-Pérez, A. Gutiérrez-Trashorras, S. Rodríguez-Artime, J.C. Ríos-Fernández, J.M. González-Caballín, Optimization of the propulsion plant of a liquefied natural gas transport ship, Energy Convers. Manag. 224 (2020) 113398.
[9] G. Livanos, G. Theotokatos, D. Pagonis, Techno-economic investigation of alternative propulsion plants for ferries and roro ships, Energy Convers. Manag. 79 (2014) 640–651.
[10] A. Dotto, U. Campora, F. Satta, Feasibility study of an integrated COGES-DF engine power plant in LNG propulsion for a cruise-ferry, Energy Convers. Manag. 245 (2021) 114602.
[11] L. Smith, H. Karim, S. Etemad, W.C. Pfefferle, The gas turbine handbook, (2006).
[12] C.A. Merz, T.J. Pakula, The design and operational characteristics of a combined cycle marine powerplant, Vol. ASME 1972 International Gas Turbine and Fluids Engineering Conference and Products Show of Turbo Expo: Power for Land, Sea, and Ai, 1972.10.1115/72-GT-90.
[13] F. Haglind, A review on the use of gas and steam turbine combined cycles as prime movers for large ships. Part II: previous work and implications, Energy Convers. Manag. 49 (2008) 3468–3475.
[14] G. Benvenuto, U. Campora, M. Laviola, Assessment of steam cycle layouts for cogas ship propulsion systems, Proceedings of the 2th International Conference on Maritime Technology and Engineering, (2014), pp. 743–754.
[15] M. Altosole, G. Dubbioso, M. Figari, M. Viviani, S. Michetti, A. Millerani Trapani, Simulation of the dynamic behaviour of a codlag propulsion plant, in: Proceedings WARSHIP 2010 Conference: Advanced Technologies in Naval Design and Construction, 2010, 9–10.

[16] M. Altosole, G. Benvenuto, M. Figari, U. Campora, A. Bagnasco, S. D′Arco, M. Giuliano, V. Giuffra, A. Spadoni, A. Zanichelli, S. Michetti, M. Ratto, Real time simulation of the propulsion plant dynamic behaviour of the aircraft carrier "cavour", Conference Proceedings of the Institute of Marine Engineering, Science and Technology - INEC 2008: Embracing the Future (2008).
[17] D. Barsi, C. Costa, F. Satta, P. Zunino, V. Sergeev, Feasibility of mini combined cycles for naval applications, MATEC Web of Conferences, Vol. 245 EDP Sciences, 2018, p. 07008.
[18] D. Barsi, M. Luzzi, F. Satta, P. Zunino, On the possible introduction of mini gas turbine cycles onboard ships for heat and power generation, 568, Energies 14 (3) (2021) 1–12.
[19] M.T. Schobeiri, M.S. Attia, C. Lippke, Getran: a generic, modularly structured computer code for simulation of dynamic behavior of aero- and power generation gas turbine engines, J. Eng. Gas. Turbines Power-Trans. Asme 116 (1994) 483–494.
[20] G. Hou, L. Gong, C. Huang, J. hang Zhang, Fuzzy modeling and fast model predictive control of gas turbine system, Energy 200 (2020) 117465.
[21] J. Rùa, L.O. Nord, Optimal control of flexible natural gas combined cycles with stress monitoring: linear vs nonlinear model predictive control, Appl. Energy 265 (2020) 114820.
[22] S. Kim, K. soon Kim, C. Son, A new transient performance adaptation method for an aero gas turbine engine, Energy 193 (2020) 116752.
[23] E. Tsoutsanis, N. Meskin, M.A. Benammar, K. Khorasani, A component map tuning method for performance prediction and diagnostics of gas turbine compressors, Appl. Energy 135 (2014) 572–585.
[24] N. Hadroug, A. Hafaifa, A. Kouzou, A. Chaibet, Dynamic model linearization of two shafts gas turbine via their input/output data around the equilibrium points, Energy 120 (2017) 488–497.
[25] C. Wang, Y. Li, B.Y. Yang, Transient performance simulation of aircraft engine integrated with fuel and control systems, Appl. Therm. Eng. 114 (2017) 1029–1037.
[26] A. Mehrpanahi, G. Payganeh, M. Arbabtafti, Dynamic modeling of an industrial gas turbine in loading and unloading conditions using a gray box method, Energy 120 (2017) 1012–1024.
[27] H. Asgari, X. Chen, M. Morini, M. Pinelli, R. Sainudiin, P.R. Spina, M. Venturini, Narx models for simulation of the start-up operation of a single-shaft gas turbine, Appl. Therm. Eng. 93 (2016) 368–376.
[28] U. Campora, M.A. Capelli, C. Cravero, R. Zaccone, Metamodels of a gas turbine powered marine propulsion system for simulation and diagnostic purposes, J. Nav. Archit. Mar. Eng. 12 (2015) 1–14.
[29] H. Zhao, H. Zhang, L. Zou, R.C. Martineau, A strongly coupled reactor core isolation cooling system model for extended station black-out analyses, Tech. rep., Idaho National Lab.(INL), Idaho Falls, ID (United States) (2015).
[30] F. Alobaid, R. Postler, J. Ströhle, B. Epple, H.-G. Kim, Modeling and investigation start-up procedures of a combined cycle power plant, Appl. Energy 85 (2008) 1173–1189.
[31] M. Pondini, V. Colla, A. Signorini, Models of control valve and actuation system for dynamics analysis of steam turbines, Appl. Energy 207 (2017) 208–217.
[32] J. Beiron, R.M. Montañés, F. Normann, F. Johnsson, Flexible operation of a combined cycle cogeneration plant – a techno-economic assessment, Appl. Energy 278 (2020) 115630.
[33] N. Mertens, F. Alobaid, R. Starkloff, B. Epple, H.-G. Kim, Comparative investigation of drum-type and once-through heat recovery steam generator during start-up, Appl. Energy 144 (2015) 250–260.
[34] Z. Sun, L. Gao, J. Wang, Y. Dai, Dynamic optimal design of a power generation system utilizing industrial waste heat considering parameter fluctuations of exhaust gas, Energy 44 (2012) 1035–1043.
[35] A. Traverso, Transeo code for the dynamic performance simulation of micro gas turbine cycles, Vol. Volume 5: Turbo Expo 2005 of Turbo Expo: Power for Land, Sea, and Air, 2005, 45–54.
[36] M.P. Boyce, Handbook for cogeneration and combined cycle power plants, (2010).
[37] S. Basu, A.K. Debnath, Power plant instrumentation and control handbook: a guide to thermal power plants, Academic Press, 2014.
[38] A. Benato, A. Stoppato, S. Bracco, Combined cycle power plants: a comparison between two different dynamic models to evaluate transient behaviour and residual life, Energy Convers. Manag. 87 (2014) 1269–1280.
[39] C. Nuchturee, T. Li, H. Xia, Energy efficiency of integrated electric propulsion for ships – a review, Renew. Sustain. Energy Rev. 134 (110145) (2020) 1–25.
[40] MAN, MAN 51/60DF IMO Tier II, IMO Tier III Project Guide-Marine (2015) 411–414.
[41] M. Altosole, G. Benvenuto, U. Campora, Numerical modelling of the engines governors of a CODLAG propulsion plant, in: International Conference on Marine Sciences and Technologies, 2010.
[42] L.O. Nord, R.M. Montañés, Compact steam bottoming cycles: model validation with plant data and evaluation of control strategies for fast load changes, Appl. Therm. Eng. 142 (2018) 334–345.
[43] J. Klapproth, M. Miller, D. Parker, Aerodynamic development and performance of the cf6–6/lm2500 compressor, in: 4th International Symposium on Air Breathing Engines, 1979, 7030.
[44] W. Zhu, X. Ren, X. Li, C. Gu, Z. Liu, Z. Yan, H. Zhu, T. Zhang, Improvement of part-load performance of gas turbine by adjusting compressor inlet air temperature and igv opening, Front. Energy (2021) 1–17.
[45] Y. Yang, Z. Bai, G. Zhang, Y. Li, Z. Wang, G. Yu, Design/off-design performance simulation and discussion for the gas turbine combined cycle with inlet air heating, Energy 178 (2019) 386–399.
[46] O. Purba, F. Zhultriza, Inlet guide vane tracking effectiveness at various compressor efficiency of gas turbine, IOP Conference Series: Materials Science and Engineering, Vol. 1096 IOP Publishing, 2021, p. 012088.
[47] M.B. Hashmi, T.A. Lemma, Z.A. Abdul Karim, Investigation of the combined effect of variable inlet guide vane drift, fouling, and inlet air cooling on gas turbine performance, Entropy 21 (12) (2019) 1186.
[48] F. Haglind, Variable geometry gas turbines for improving the part-load performance of marine combined cycles – gas turbine performance, Energy 35 (2010) 562–570.
[49] GasTurb GmbH, GasTurb 14 User Manual(2022).
[50] R. Kurz, K. Brun, et al., Gas turbine performance-what makes the map?, in: Proceedings of the 29th Turbomachinery Symposium, Texas A&M University. Turbomachinery Laboratories, 2000.
[51] F. Baldi, F. Ahlgren, T.-V. Nguyen, M. Thern, K. Andersson, Energy and exergy analysis of a cruise ship, Energies 11 (10) (2018) 2508.
[52] R. Bachmann, H. Nielsen, J. Warner, R. Kehlhofer, Combined-cycle gas & steam turbine power plants, PennWell Publishing Company,, Tulsa, OK, 1999.
[53] A. Gimelli, M. Muccillo, Regulation problems of combined cycle gas-steam turbine power plant in a liberalized market: Part I - experimental investigation and energetic analysis, Int. Rev. Model. Simul. 9 (2016) 295–305.
[54] R. Carapellucci, L. Giordano, Studying the effects of combining internal and external heat recovery on techno-economic performances of gas-steam power plants, Energy Convers. Manag. 107 (2016) 34–42.
[55] Available at: 〈https://www.fincantieri.com/en/products-and-services/systems-components/turbines/〉.2023.
[56] A.S. Karakurt, Performance analysis of a steam turbine power plant at part load conditions, J. Therm. Eng. 3 (2) (2017) 1121–1128.
[57] T. Brown, S.S. Cook, F. Gardner, Steam and gas turbines for marine propulsion, Proc. Inst. Mech. Eng. 157 (1) (1947) 175–183.